Cauer Circuit Representation of the Homogenized Eddy-Current Field Based on the Legendre Expansion for a Magnetic Sheet

AUTHOR(S):

Shindo, Yuji; Miyazaki, Tatsuya; Matsuo, Tetsuji

Cauer Circuit Representation of the Homogenized Eddy-Current Field Based on the Legendre Expansion for a Magnetic Sheet

Yuji Shindo[1], Tatsuya Miyazaki[2], and Tetsuji Matsuo[2], *Member IEEE*

[1] Kawasaki Heavy Industries, Ltd., Akashi, 673-8666, Japan, shindo_yuji@khi.co.jp
[2] Graduate School of Engineering, Kyoto University, 615-8510, Japan, matsuo.tetsuji.5u@kyoto-u.ac.jp

Using the Legendre expansion of the magnetic field distribution, we derive the standard Cauer circuit representation of the frequency-dependent properties of magnetic sheets and discuss its physical meaning. The representation of nonlinear inductors is derived so as to apply the Cauer circuit in the dynamic hysteresis modeling of silicon steel. This circuit accurately reconstructs the hysteretic property under pulse-width-modulation excitation using only one or two hysteretic elements.

***Index Terms*—Cauer realization, dynamic hysteresis, Legendre polynomial, pulse width modulation.**

I. Introduction

Progress in the semiconductor technology has resulted in advanced power control with high-frequency switching operations that induce complex dynamic hysteretic magnetic fields in iron cores. Minor hysteresis loops and eddy-current fields with thin skin depths are significant within these cores.

Several homogenization methods [1]–[5] have been developed for efficient analysis of the laminated cores that avoid the finite-element division along the stacking direction of the silicon steel sheets. However, an accurate evaluation of the eddy-current field in sheets displaying nonlinear magnetic properties is difficult without a one-dimensional sub-analysis along the sheet-thickness direction [1]–[4]. The sub-analysis requires the division along the thickness direction to skin depth scale. For example, if the skin depth is 0.5 mm at 50 Hz, it becomes 0.05 and 0.01 mm at 5 kHz and 125 kHz, respectively, resulting in a fine element grid for the steel sheet.

An efficient representation of the frequency-dependent properties of magnetic sheets is achieved using the standard and physical Cauer circuit representations [5]–[7] based on the linear eddy-current theory. Although the standard Cauer circuit is obtained directly from the linear theory, it has not been applied to nonlinear eddy-current analysis because its physical meaning is unclear. In contrast, the physical Cauer circuit has been used in nonlinear analysis because of its clear physical meaning. In the nonlinear case, however, the physical Cauer circuit requires more inductive elements than expected from the linear circuit, even after circuit optimization [5].

Ref. [8] discusses the meaning of the truncated standard Cauer circuit with two inductors comparing the homogenization method developed in Ref. [2], [3] based on the Legendre expansion. Here we derive the standard Cauer circuit directly from the Legendre expansion for the magnetic field to consider the physical meaning of this circuit. The representation of a nonlinear inductor is derived to apply the standard Cauer circuit to the dynamic hysteresis modeling of a steel sheet.

Manuscript received April 1, 2015; revised May 15, 2015 and June 1, 2015; accepted July 1, 2015. Date of publication July 10, 2015; date of current version July 31, 2015. Corresponding author: T. Matsuo (e-mail: matsuo.tetsuji.5u@kyoto-u.ac.jp).

Color versions of one or more of the figures in this paper are available online at http://ieeexplore.ieee.org.

Digital Object Identifier (inserted by IEEE).

II. Derivation of Cauer Circuit by Legendre Expansion

A. Cauer realization

The magnetic field in the steel sheet of thickness d is governed by

$$\frac{\partial^2 H}{\partial z^2} = \sigma \frac{\partial B}{\partial t}, \quad \left(-\frac{d}{2} \le z \le \frac{d}{2} \right), \tag{1}$$

where σ is the conductivity. A linear eddy-current theory for the magnetic sheet gives the relationship between the average magnetic flux density B_{av} and the surface magnetic field H_{s} as

$$\frac{B_{\mathrm{av}}}{H_{\mathrm{s}}} = \mu \frac{2}{kd} \tan\left(\frac{kd}{2} \right) = \mu \frac{2}{\mathrm{j}kd} \tanh\left(\frac{\mathrm{j}kd}{2} \right), \tag{2}$$

where $k = (-\mathrm{j}\omega\sigma\mu)^{1/2}$, ω is the angular frequency, and μ the permeability. By expanding $\tan(kd/2)$ or $\tanh(\mathrm{j}kd/2)$, (2) is represented by the infinite *RL* ladder circuit [6], [7] (see Fig. 1), where μ and $4/\sigma d^2$ are replaced by the inductance L and resistance R, respectively. This circuit is called the standard Cauer circuit.

B. Legendre expansion

Refs. [2], [3] describes a homogenization method where the magnetic flux density distribution along the thickness direction is expanded as Legendre polynomials [9] $P_{2n}(x)$ ($-1 \le x \le 1$, $n = 0, 1, \ldots$) as

$$B(t,z) = b_0(t) P_0\left(\frac{2z}{d} \right) + b_2(t) P_2\left(\frac{2z}{d} \right) + b_4(t) P_4\left(\frac{2z}{d} \right) + \cdots. \tag{3}$$

This subsection derives the standard Cauer circuit using (3) and the orthogonality of the Legendre polynomials below:

$$\int_{-1}^{1} P_m(x) P_n(x) \mathrm{d}x = \begin{cases} 0 & (m \ne n) \\ 2/(2m+1) & (m = n) \end{cases}. \tag{4}$$

By defining

$$\boldsymbol{P} = \left[P_0\left(\frac{2z}{d} \right), P_2\left(\frac{2z}{d} \right), P_4\left(\frac{2z}{d} \right), \ldots \right]^{\mathrm{T}}, \tag{5}$$

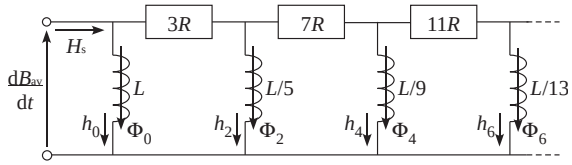

Fig. 1. Standard Cauer circuit.

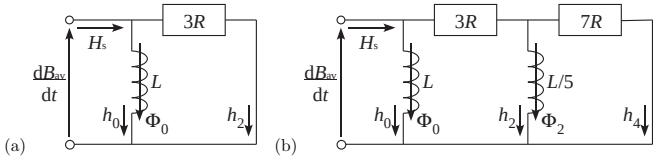

Fig. 2. Truncated standard Cauer circuit: (a) with one inductor and (b) with two inductors.

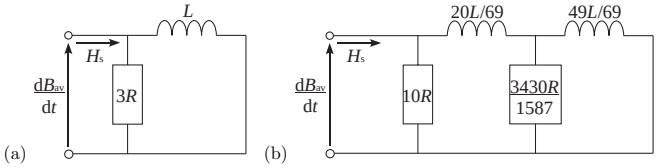

Fig. 3. Physical Cauer circuit: (a) with one inductor and (b) with two inductors.

$$\boldsymbol{h}=[h_0(t),h_2(t),h_4(t),\cdots]^{\mathrm{T}}=\frac{1}{\mu}[b_0(t),b_2(t),b_4(t),\cdots]^{\mathrm{T}}, \quad (6)$$

(1) is rewritten as

$$\boldsymbol{h}^{\mathrm{T}}\frac{\partial^2\boldsymbol{P}}{\partial z^2}=\sigma\frac{\mathrm{d}(\mu\boldsymbol{h}^{\mathrm{T}})}{\mathrm{d}t}\boldsymbol{P}. \quad (7)$$

Using the relations,

$$\frac{\mathrm{d}P_{2n}(x)}{\mathrm{d}x}=(4n-1)P_{2n-1}(x)+(4n-5)P_{2n-3}(x)+\cdots+3P_1(x),$$
$$\frac{\mathrm{d}P_{2n+1}(x)}{\mathrm{d}x}=(4n+1)P_{2n}(x)+(4n-3)P_{2n-2}(x)+\cdots+P_0(x), \quad (8)$$

(7) is written

$$[\sigma\frac{\mathrm{d}(\mu\boldsymbol{h}^{\mathrm{T}})}{\mathrm{d}t}-\frac{4}{d^2}\boldsymbol{h}^{\mathrm{T}}\boldsymbol{G}\boldsymbol{F}]\boldsymbol{P}=0 \quad (9)$$

where

$$\boldsymbol{F}=\mathrm{diag}(1,5,9,\cdots), \quad (10)$$

$$\boldsymbol{G}=\begin{bmatrix}0 & 0 & 0 & 0 & \cdots\\ 3 & 0 & 0 & 0 & \cdots\\ 3+7 & 7 & 0 & 0 & \cdots\\ 3+7+11 & 7+11 & 11 & 0 & \cdots\\ \vdots & \vdots & \vdots & \vdots & \ddots\end{bmatrix}. \quad (11)$$

From (9) and the orthogonality (4),

$$\boldsymbol{F}^{-1}\frac{\mathrm{d}(L\boldsymbol{h})}{\mathrm{d}t}-\frac{4}{\sigma d^2}\boldsymbol{G}^{\mathrm{T}}\boldsymbol{h}=0 \quad (12)$$

is obtained. As the surface magnetic field H_s is given as

$$H_s(t)=\frac{1}{\mu}B(t,\frac{d}{2})=h_0(t)+h_2(t)+h_4(t)+\cdots, \quad (13)$$

(12) describes the equation of state for the standard Cauer circuit of Fig. 1, where

$$\Phi_{2n}(t)=\frac{b_{2n}(t)}{4n+1}. \quad (14)$$

The physical meaning of the standard Cauer circuit was discussed in [8] and is given as follows. When the frequency is low, $h_0(t)$ ($\approx H_s(t)$) is the dominant current and the flux change $\mathrm{d}\Phi_0/\mathrm{d}t = L\mathrm{d}h_0/\mathrm{d}t$ induces an eddy-current $h_2(t) \approx (\mathrm{d}B_{\mathrm{av}}/\mathrm{d}t)/(3R)$. Accordingly, the magnetic flux $\Phi_2 = (L/5)h_2$ is regarded as the secondary flux generated by the induced current h_2. This explanation is supported by the Legendre expansion. The uniformly distributed magnetic flux density b_0P_0 induces the eddy current distributed linearly along the z-direction, which yields the parabolically distributed b_2P_2.

Furthermore, (3), (6), and the orthogonality (4) give the magnetic energy $w(t)$ per unit volume as

$$w(t)=\frac{1}{d}\cdot\frac{1}{2\mu}\int_{-d/2}^{d/2}B^2(t,z)\mathrm{d}z$$
$$=\frac{1}{d}\cdot\frac{\mu}{2}\sum_{n=0}^{\infty}\int_{-d/2}^{d/2}h_{2n}^2(t)P_{2n}^2\left(\frac{2z}{d}\right)\mathrm{d}z=\frac{1}{2}\cdot\sum_{n=0}^{\infty}\frac{L}{4n+1}h_{2n}^2(t) \quad (15)$$

Note that the energy associated with the flux distribution $\mu h_{2n}(t)P_{2n}(2z/d)$ in the magnetic sheet coincides with the energy stored in the inductor $L/(4n+1)$ of the Cauer circuit. The physical magnetic energy in the magnetic sheet is conserved in the Cauer circuit representation.

By truncating the standard Cauer circuit (Fig. 2), they can be converted to equivalent types of RL ladder circuits (Fig. 3). These circuits are called physical Cauer circuits because the ratio of the inductances corresponds to the nonuniform physical division [5]–[7] of the half thickness $d/2$. The truncated circuit shown in Fig. 2(a) is the same as the circuit in Fig. 3(a), which in classical eddy-current theory represents

$$H_s(t)=\frac{1}{\mu}B_{\mathrm{av}}(t)+\frac{\sigma d^2}{12}\frac{\mathrm{d}B_{\mathrm{av}}}{\mathrm{d}t}. \quad (16)$$

The equivalence of truncated standard Cauer circuit to the homogenization method in [2], [3] is proved in the Appendix.

When the Cauer circuit is truncated with $(N+1)$ pairs of L / $(4n+1)$ and $(4n+3)R$ (n = 0, …, N), its impedance at high frequency ($\omega >> R/L$) asymptotically becomes $3R + 7R + \ldots + (4N+3)R = (N+1)(2N+3)R$ because the inductors are approximately open-circuited. This means that the iron loss for the sinusoidal B with amplitude B_{m} becomes

$$P_N\approx\frac{\omega^2B_m^2}{2(N+1)(2N+3)R}\quad(\omega L>>R). \quad (17)$$

From (2), the infinite Cauer circuit gives the iron loss as

$$P\approx\frac{\omega^{3/2}B_m^2}{\sqrt{8RL}}\quad(\omega L>>R). \quad (18)$$

Equating (17) with (18), the frequency range where the truncated Cauer circuit is applicable is evaluated as

$$\omega<\omega_N=\frac{(N+1)^2(2N+3)^2R}{2L}. \quad (19)$$

Equation (19) implies that a small increase of N results in a large increase of frequency range.

C. Nonlinear inductors

If the static magnetic property of a steel sheet has nonlinearity represented by $H_s = H_{\mathrm{DC}}(B_{\mathrm{av}})$, the first inductor L is replaced by relation $h_0 = H_{\mathrm{DC}}(\Phi_0)$. Magnetic fluxes Φ_2, Φ_4,

… can be regarded as corrections to flux Φ_0. If the flux correction is small and H_{DC} is not a hysteretic function, one obtains

$$H(t,z) = H_{DC}\left(b_0(t) + b_2(t)P_2\left(\frac{2z}{d}\right) + b_4(t)P_4\left(\frac{2z}{d}\right) + \cdots\right) \quad (20)$$
$$\approx H_{DC}(b_0(t)) + \frac{1}{\mu_d}\left(b_2(t)P_2\left(\frac{2z}{d}\right) + b_4(t)P_4\left(\frac{2z}{d}\right) + \cdots\right)$$

where $\mu_d = [dH_{DC}(\Phi_0)/d\Phi_0]^{-1}$ is the differential permeability. By setting

$$\boldsymbol{h} = \frac{1}{\mu_d}[b_0(t), b_2(t), b_4(t), \cdots]^T \quad (21)$$

and replacing μ and L by μ_d, (7), (9), and consequently (12) hold. By setting,

$$h_0(t) = H_{DC}(b_0(t)),\ h_{2n}(t) = b_{2n}(t)/\mu_d \quad (n = 1, 2, \ldots). \quad (22)$$

(12), (13), and (14) describes the equation of state for the standard Cauer circuit (Fig. 1) with the state variables Φ_{2n} (n = 0, 1, …), where Lh_0 is replaced by Φ_0 satisfying $h_0 = H_{DC}(\Phi_0)$. The relation between h_{2n} and Φ_{2n} (n = 1, 2, …) is given as

$$h_{2n}(t) = (4n+1)\Phi_{2n}(t)/\mu_d, \quad (23)$$

where μ_d is a function of $b_0 = \Phi_0$.

If H_{DC} is hysteretic, however, the linear approximation (20) does not hold because the past history of the input perturbation affects the present hysteretic output. Instead of using (20), Ref. [8] proposed a finite difference approximation

$$h_{2n} = \frac{4n+1}{\varepsilon}[H_{DC}(\Phi_0 + \varepsilon\Phi_{2n}) - H_{DC}(\Phi_0)], \quad (24)$$

where ε is a constant and H_{DC} is affected by the history of Φ_0 and $\Phi_0+\varepsilon\Phi_{2n}$.

To represent the nonlinear inductor $L/(4n+1)$ (n = 1, 2, …), we propose a rough approximation using (20). By neglecting hysteresis, H_{DC} is approximated by a single-valued function $H_0(B)$ to give the differential permeability as $\mu_d = [dH_0(\Phi_0)/d\Phi_0]^{-1}$. To approximate H_{DC}, two types of single-valued functions below are examined:

$$H_0 = H_{ave}(B) = \frac{1}{2}[H_+(B) + H_-(B)], \quad (25)$$

$$H_0 = H_{rev}(B), \quad (26)$$

where $H_{ave}(B)$ is given by the average of ascending curve $H_+(B)$ and descending curve $H_-(B)$ of the major loop of $H_{DC}(B)$. The second function $H_{rev}(B)$ is the reversible component of $H_{DC}(B)$ used to approximate $H_{DC}(B)$ under the pulse-width-modulation (PWM) excitation. If the fundamental frequency of the PWM waveform is low, the fundamental component is not affected by elements of $L/(4n+1)$ and $(4n+3)R$ ($n \geq 1$). The PWM carrier frequency yields small minor hysteresis loops, which are affected by $L/5$ and $7R$. Accordingly, μ_d can be given by the incremental permeability ($\Delta B/\Delta H$ in Fig. 4) of minor loops, which is roughly approximated by $dH_{rev}(B)/dB$.

In the physical Cauer circuit, the k-th inductor L/α_k can be replaced by the relation $h_k = H_{DC}(\alpha_k\Phi_k)$ because L/α_k corresponds to the magnetic flux passing through $1/\alpha_k$ of the sheet's thickness. A similar interpretation for inductor $L/(4n+1)$ in the standard Cauer circuit is given by $h_{2n} = H_{DC}((4n+1)\Phi_{2n})$, which does not give more accurate results than (24) [8].

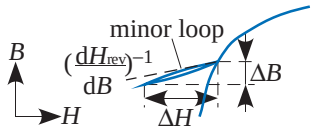

Fig. 4. Permeability for the minor B–H loop.

III. Numerical Result

B–H loops and iron losses of a non-oriented silicon steel sheet, JIS: 35A300 were measured with a single sheet tester using two-types of PWM waveforms, for which the fundamental and carrier frequencies are 50 Hz and 10 kHz. The static hysteretic property $H = H_{DC}(B)$ for the steel sheet is represented by the play model [10]. The measured B_{av} is given to simulate the surface field H_s.

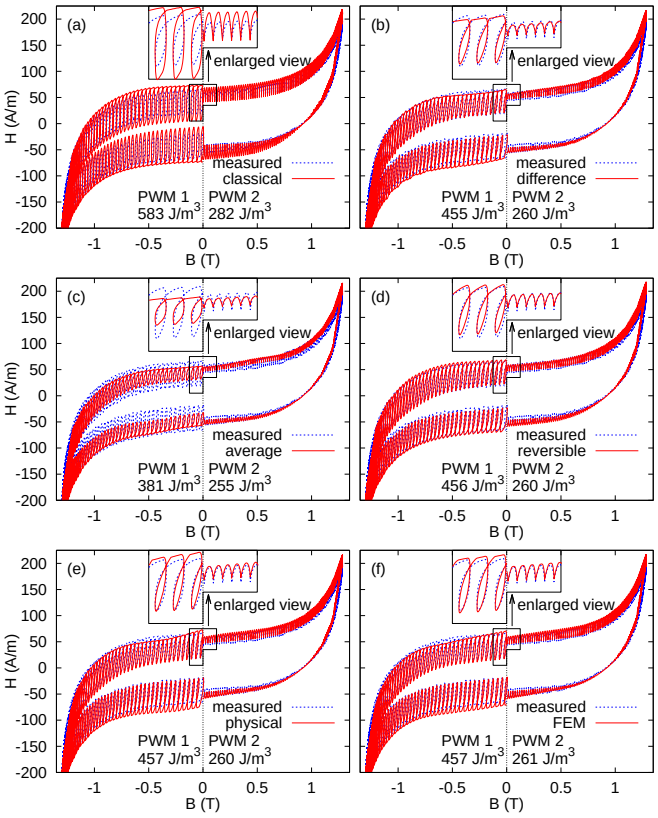

Fig. 5. Simulated B–H loops for 2 types of PWM waveforms where measured iron losses per cycle are 458 and 252 J/m^3: (a) classical eddy-current theory, (b) standard Cauer circuit with finite-difference approximation (21) with ε = 1, (c) standard Cauer circuit with average approximation, (d) standard Cauer circuit with reversible component approximation, (e) physical Cauer circuit, and (f) finite element method.

Fig. 5(a) shows the simulated B–H loops produced by the standard Cauer circuit, shown in Fig. 2(a), which is equivalent to the classical eddy-current theory. Fig. 5(b)–(d) given by the circuit shown in Fig. 2(b), where (b) the finite difference approximation (24), (c) the average approximation H_{ave}, and (d) the reversible component H_{rev} are used to represent the second inductor $L/5$. For comparison, Fig. 5(e) and (f) shows the B–H loops given by the physical Cauer circuit shown in Fig. 3(b) and the one-dimensional finite element eddy-current analysis along the z-direction with 10 first-order elements.

Assuming that Φ_{2n} is small, ε in (24) is set to 1. Fig. 5(a)–(f) presents the computed iron losses per cycle for the PWM waveforms 1 and 2, which in measurements yield 458 and 252 J/m^3. The PWM waveform 1 has 1.2 % of 200-th harmonic in B_{av} due to the carrier wave whereas the waveform 2 has 0.17 % of (400±1)-th harmonics. If the linear magnetic property is assumed with $L = 5 \times 10^{-3}$ H/m and $R = 12$ Ω/m, $\omega_0/2\pi$ and $\omega_1/2\pi$ are 1.7 and 19 kHz from (19) and the ratio of amplitude of b_2 to that of b_0 is 0.09 and 0.06 for the waveforms 1 and 2. The classical eddy-current theory overestimates the component of carrier frequency [Fig. 5(a)], because the effect of secondary flux Φ_2 is neglected even though the carrier frequency is larger than $\omega_0/2\pi$. The average approximation underestimates the minor loops [Fig. 5(c)] because the inductance $L/5$ given by $[\mathrm{d}H_{ave}(\Phi_0)/\mathrm{d}\Phi_0]^{-1}$ / 5 is too large for the minor B–H loops. In contrast, the reversible component approximation achieves an accurate representation as the finite-difference approximation and the finite-element method (FEM) because $\mathrm{d}H_{rev}(\Phi_0)/\mathrm{d}\Phi_0$ gives a good approximation for the permeability of the minor loops. Note that the standard Cauer circuit using H_{rev} requires only one hysteretic inductor whereas the Cauer circuit with the finite-difference approximation needs two hysteretic inductors, and the FEM requires as many hysteretic elements as the number of finite elements. The physical Cauer circuit with two hysteretic inductors results in a slightly inaccurate outer B–H-loop representation, which is improved by increasing the number of inductors because the physical Cauer circuit is equivalent to the nonuniformly divided FEM.

IV. Conclusion

Using the Legendre expansion of the magnetic field distribution, we derive the standard Cauer circuit representation of the frequency-dependent properties of magnetic sheets. The circuit representation provides us useful information such as the applicable frequency limitation due to the truncation. The representation of the nonlinear inductors is derived and gives accurate dynamic hysteretic properties for silicon steel under PWM excitation only with one or two hysteretic inductors.

Appendix

From (8), one obtains that

$$\int P_n(x)\mathrm{d}x = \frac{1}{2n+1}[P_{n+1}(x) - P_{n-1}(x)] \quad (n = 1, 2, \ldots). \tag{27}$$

From (27), we have

$$\iint P_{2n}(x)\mathrm{d}x\mathrm{d}x = \frac{1}{4n+1}\left[\frac{P_{2n+2}(x) - P_{2n}(x)}{4n+3} - \frac{P_{2n}(x) - P_{2n-2}(x)}{4n-1}\right],$$
$$\iint P_0(x)\mathrm{d}x\mathrm{d}x = \int P_1(x)\mathrm{d}x = [P_2(x) - P_0(x)]/3. \tag{28}$$

Using the truncated Legendre expansion

$$B(t,z) = \sum_{n=0}^{N} b_{2n}(t) P_{2n}\left(\frac{2z}{d}\right) \tag{29}$$

Ref. [2], [3] integrates (1) twice with respect to z to obtain

$$H(t,z) = \sigma\iint \frac{\mathrm{d}B(t,z)}{\mathrm{d}t}\mathrm{d}z\mathrm{d}z = \sigma\sum_{n=0}^{N}\frac{\mathrm{d}b_{2n}(t)}{\mathrm{d}t}\iint P_{2n}(\frac{2z}{d})\mathrm{d}z\mathrm{d}z. \tag{30}$$

Using (30), $H(t, z)$ is rewritten in the form

$$H(t,z) = H_s(t) + \frac{\sigma d^2}{4}\frac{\mathrm{d}b_0}{\mathrm{d}t}\frac{P_2 - P_0}{3} + \sum_{n=1}^{N}\frac{\sigma d^2}{4(4n+1)}\frac{\mathrm{d}b_{2n}}{\mathrm{d}t}\left(\frac{P_{2n+2} - P_{2n}}{4n+3} - \frac{P_{2n} - P_{2n-2}}{4n-1}\right). \tag{31}$$

If linearity is assumed for the magnetic property $H(t, z) = B(t, z)/\mu$, the orthogonality of Legendre functions leads to

$$\frac{1}{\mu}b_{2n}(t) = \frac{1}{4n+3}\frac{\sigma d^2}{4(4n+5)}\frac{\mathrm{d}b_{2n+2}}{\mathrm{d}t} - (\frac{1}{4n+3} + \frac{1}{4n-1})\frac{\sigma d^2}{4(4n+1)}\frac{\mathrm{d}b_{2n}}{\mathrm{d}t} + \frac{1}{4n-1}\frac{\sigma d^2}{4(4n-3)}\frac{\mathrm{d}b_{2n-2}}{\mathrm{d}t} \quad (1 \le n \le N)$$
$$\frac{1}{\mu}b_0(t) = H_s(t) + \frac{1}{3}\frac{\sigma d^2}{4\cdot 5}\frac{\mathrm{d}b_2}{\mathrm{d}t} - \frac{1}{3}\frac{\sigma d^2}{4}\frac{\mathrm{d}b_0}{\mathrm{d}t} \tag{32}$$

where b_{2N+2} is set to 0. Setting as in (14), (30) is rewritten as

$$\frac{4n+1}{\mu}\Phi_{2n}(t) = \frac{1}{(4n+3)R}(\frac{\mathrm{d}\Phi_{2n+2}}{\mathrm{d}t} - \frac{\mathrm{d}\Phi_{2n}}{\mathrm{d}t}) + \frac{1}{(4n-1)R}(\frac{\mathrm{d}\Phi_{2n-2}}{\mathrm{d}t} - \frac{\mathrm{d}\Phi_{2n}}{\mathrm{d}t}) \quad (1 \le n \le N),$$
$$\frac{1}{\mu}\Phi_0(t) = H_s(t) + \frac{1}{3R}(\frac{\mathrm{d}\Phi_2}{\mathrm{d}t} - \frac{\mathrm{d}\Phi_0}{\mathrm{d}t}) \tag{33}$$

where Φ_{2N+2} is set to 0. The equation of state for the standard Cauer circuit truncated with N inductors is given by (33). Using the linear approximation (20), the weak form of the constitutive equation proposed in [3] for the nonlinear property is similarly represented by the standard Cauer circuit.

References

[1] O. Bottauscio, M. Chiampi, D. Chiarabaglio, "Advanced model of laminated magnetic cores for two-dimensional field analysis," *IEEE Trans. Magn.*, vol. 36, pp. 561–573, May 2000.
[2] J. Gyselinck, P. Dular, "A time-domain homogenization technique for laminated iron cores in 3-D finite-element models," *IEEE Trans. Magn.*, vol. 40, pp. 856–859, Mar. 2004.
[3] J. Gyselinck, R.V. Sabariego, P. Dular, "A nonlinear time-domain homogenization technique for laminated iron cores in three-dimensional finite-element models," *IEEE Trans. Magn.*, vol. 42, pp. 763–766,Apr. 2006.
[4] I. Niyonzima, R.V. Sabariego, P. Dular, F. Henrotte, C. Geuzaine, "Computational homogenization for laminated ferromagnetic cores in magnetodynamics," *IEEE Trans. Magn.*, vol. 49, pp. 2049–2052, May 2013.
[5] J.H. Krah, "Optimum discretization of a physical Cauer circuit," *IEEE Trans. Magn.*, vol. 41, pp. 1444-1447, May 2005.
[6] E. Tarasiewicz, A.S. Morched, A. Narang, E.P. Dick, "Frequency dependent eddy current models for nonlinear iron cores," *IEEE Trans. Power Syst.*, vol. 8, pp. 588–597, May 1993.
[7] Y. Shindo, O. Noro, "Simple circuit simulation models for eddy current in magnetic sheets and wires," *IEEJ Trans. FM*, vol.134, pp. 173–181, Apr. 2014.
[8] T. Miyazaki, T. Mifune, T. Matsuo, Y. Shindo, Y. Takahashi, K. Fujiwara, "Equivalent circuit modeling of dynamic hysteretic property of silicon steel sheet under pulse width modulation excitation," *J. Appl. Phys.* vol. 117, 17D110, 2015.
[9] W. W. Bell, *Special functions for scientists and engineers*, New York: Dover, 2004, pp. 42–91.
[10] T. Matsuo, M. Shimasaki, "An identification method of play model with input-dependent shape function," *IEEE Trans. Magn.*, vol. 41, pp. 3112-3114, Oct. 2005.